Low-temperature exchange coupling between Fe_2O_3 and $FeTiO_3$: Insight into the mechanism of giant exchange bias in a natural nanoscale intergrowth

Richard J. Harrison,[1,*] Suzanne A. McEnroe,[2] Peter Robinson,[2] Brian Carter-Stiglitz,[3] Erika J. Palin,[1] and Takeshi Kasama[4]
[1]*Department of Earth Sciences, University of Cambridge, Downing Street, Cambridge CB2 3EQ, United Kingdom*
[2]*Geological Survey of Norway, N-7491 Trondheim, Norway*
[3]*Institute for Rock Magnetism, Newton Horace Winchell School of Earth Sciences, University of Minnesota, Minneapolis 55455, USA*
[4]*Department of Materials Science, University of Cambridge, Pembroke Street, Cambridge, United Kingdom, CB2 3QZ*
(Received 12 May 2007; revised manuscript received 2 August 2007; published 28 November 2007)

Exchange bias (>1 T at 10 K) has been observed in natural sample of Fe_2O_3 containing abundant nanoscale exsolution lamellae of $FeTiO_3$. Exchange bias is first observed below the Néel temperature of $FeTiO_3$ (55 K). Possible interface magnetic structures are explored within the framework of a classical Heisenberg model using Monte Carlo simulations. The simulations predict a threshold value of the Fe_2O_3 anisotropy constant, below which Fe^{3+} spins become tilted out of the basal plane in the vicinity of the interfaces. This tilting creates a *c*-axis component of magnetization in the Fe_2O_3 host that couples to the *c*-axis magnetization of the $FeTiO_3$ lamellae. Exchange interactions across the interfaces are frustrated when the $FeTiO_3$ lamellae contain an even number of Fe^{2+} layers, resulting in zero net exchange bias. Lamellae containing an odd number of Fe^{2+} layers, however, are negatively exchange coupled to the Fe_2O_3 host across both (001) bounding surfaces, and are the dominant source of exchange bias. Exchange bias is observed whenever there is a significant *c*-axis component to both the Fe_2O_3 magnetization and the applied field. An exchange bias of 0.9 T was obtained with an anisotropy constant of 0.1 K.

DOI: 10.1103/PhysRevB.76.174436 PACS number(s): 75.10.Hk, 91.25.F−, 91.60.Pn, 75.75.+a

I. INTRODUCTION

The magnetic properties of titanohematite ($Fe_{1-x}Ti_xO_3$) are profoundly influenced by nanoscale microstructures associated with subsolvus exsolution and cation ordering.[1] Slowly cooled rocks containing nanoscale exsolution microstrucures have strong and extremely stable magnetic remanence, suggesting an explanation for some magnetic anomalies in the deep crust and on planetary bodies that no longer retain a magnetic field, such as Mars.[2–7] This remanence has been attributed to a stable defect moment originating from spin imbalance at the coherent interfaces between nanoscale Fe_2O_3 (hematite) and $FeTiO_3$ (ilmenite) exsolution lamellae.[8,9] Rapidly cooled members of the $Fe_{1-x}Ti_xO_3$ solid solution, on the other hand, are well known for their ability to acquire self-reversed thermoremanent magnetization.[10] This phenomenon is related to the presence of fine-scale antiphase domains that form on cooling through a cation-ordering phase transition.[11]

The discovery of giant exchange bias (EB) at temperatures below 55 K in a natural titanohematite from the Modum district, South Norway has been reported recently.[12] Imparting a positive saturation isothermal remanent magnetization (SIRM) at room temperature, followed by zero-field cooling to 20 K, causes a large negative shift of the hysteresis loop along both the horizontal and vertical axes [Fig. 1(a)]. Imparting a negative SIRM at room temperature results in a positive shift of the hysteresis loop at 20 K [Fig. 1(b)]. Demagnetizing the sample by exposure to a rapidly alternating magnetic field at room temperature leads to a perfectly symmetrical hysteresis loop at 20 K [Fig. 1(c)]. The unusual appearance of the hysteresis loops is caused by the superposition of a hysteretic component of magnetization (associated with Fe_2O_3) and a quasilinear component of magnetization (associated with antiferromagnetic $FeTiO_3$). The hysteretic component can be isolated by subtracting the lower branch of the hysteresis curve from the upper branch [Fig. 1(d)]. The position of the peak in the resulting difference curve corresponds to the EB field. This field approaches a value of 1 T at 20 K [Fig. 1(e)] and >1 T at 10 K, where only a minor hysteresis loop was obtainable in the maximum field applied of 1.5 T. Measurements performed in fields up to 7 T indicate that the EB field is 1.3 T at 10 K.[12] The size of the exchange-bias field is orders of magnitude larger than that observed in other exchange-bias systems involving Fe_2O_3.[13,14] Although this is one of the highest ever reported EB fields, its magnitude is not surprising given the small magnetization of Fe_2O_3. A more useful estimate of EB strength is the interface energy $E_A=0.52$ erg/cm^2,[12] which is larger than 95% of the technically synthesized materials reported in Table II of Nogues and Schuller.[15,16] It should be noted that the appearance of EB after zero-field cooling indicates that EB is controlled by the remanent magnetization of the Fe_2O_3 host, rather than the magnitude of the cooling field.

EB has been studied extensively from both experimental and theoretical perspectives, due to its important role in the design of giant magnetoresistive devices for magnetic storage and spintronics applications.[15,17–23] The vast majority of studies have focused on EB systems comprising a ferromagnetic (FM) thin film in contact with an antiferromagnetic (AFM) substrate. Modeling EB in such systems is complicated by a number of issues, including (a) the crystallographic and magnetic structures of the FM and/or AFM interface,[24] (b) the formation of magnetic domains within the FM and/or AFM phases,[25] and (c) the effect of interface roughness.[26] EB in titanohematite, on the other hand, is related to a coherent intergrowth of AFM $FeTiO_3$ lamellae

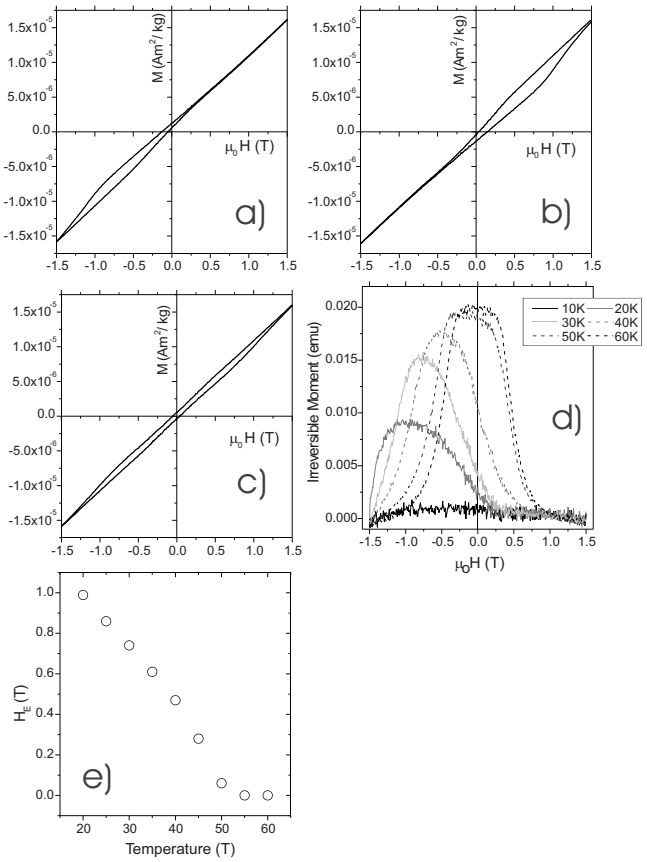

FIG. 1. Hysteresis loops [(a)–(c)] measured at 20 K after zero-field cooling and after (a) imparting a positive room-temperature remanence, (b) imparting a negative room-temperature remanence, and (c) completely demagnetizing the sample at room temperature. (d) The lower hysteresis branch subtracted from the upper branch in the case of negative exchange bias for six temperatures. The location of the center of each peak gives the magnitude of the exchange-bias field. (e) EB shift deduced from (d) as a function of temperature.

within a canted AFM Fe_2O_3 host, formed through a natural process of phase separation during slow cooling (Fig. 2). TEM observations show two generations of nanoscale exsolution lamellae [Fig. 2(a)], both identified as $FeTiO_3$ by selected-area diffraction patterns and energy-filtered imaging [Fig. 2(b)]. First-generation $FeTiO_3$ lamellae are ~10–20 nm wide, and are surrounded by a 5–10 nm region of homogeneous Fe_2O_3 host ["precipitate-free zone" in Fig. 2(c)]. Outside the precipitate-free zone, the Fe_2O_3 contains abundant, much-finer-scale $FeTiO_3$ lamellae, appearing as thin white lines (oriented ~ north east) surrounded by dark coherency strain shadows in Fig. 2(c). The region in the black square is shown at higher magnification in the inset. The black arrows indicate the positions of several fine-scale lamellae. The scale bar is 1.4 nm, corresponding to the *c* unit-cell dimension of $FeTiO_3$. Many fine-scale ilmenite lamellae are ~10 nm long and less than one *c* dimension thick. Hence, this sample provides a unique opportunity to study EB in a system where the crystal, chemical, and magnetic structures of the interface region are well established (Ref. 1) and the issues of interface roughness and domain

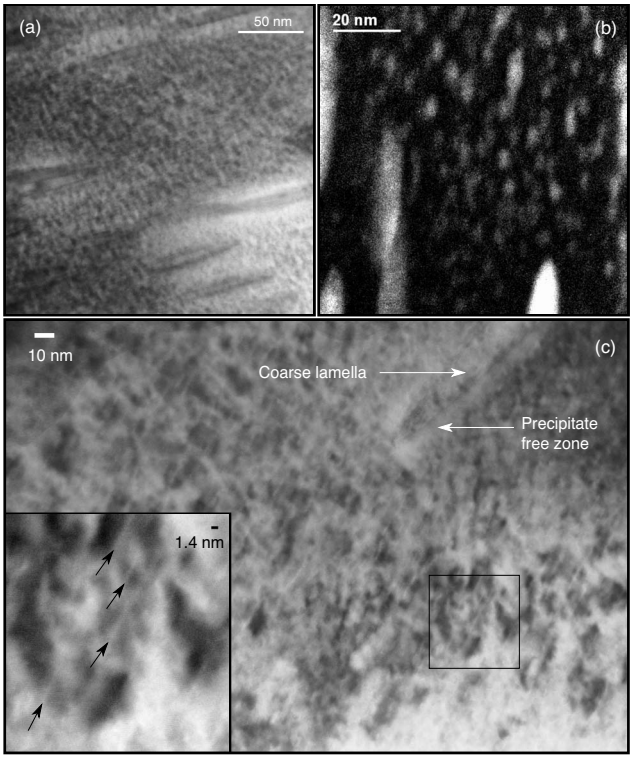

FIG. 2. (a) Bright-field TEM micrograph of the titanohematite host, showing first generation lamellae surrounded by abundant fine-scale second generation lamellae. (b) Ti chemical map of a similar area to (a) obtained using energy-filtered imaging. Bright regions are rich in Ti and were identified as $FeTiO_3$ by selected-area electron diffraction. (c) Higher magnification bright-field micrograph of first and second generation lamellae. A relatively large $FeTiO_3$ lamella surrounded by a precipitate-free zone is indicated in the upper right by the white arrows. The contrast observed in the remaining host is due to the coherency strain associated with ~1 nm thick precipitates of $FeTiO_3$. These are more clearly seen in the inset, which is an enlargement of the region indicated by the black square. The $FeTiO_3$ precipitates appear as thin white lines, indicated by the black arrows.

wall formation are reduced by the coherency and length scale of the microstructure.

II. IDEALIZED MAGNETIC STRUCTURE OF AN Fe_2O_3-$FeTiO_3$ INTERGROWTH

Figure 3 is a schematic illustration of the magnetic structure that would be obtained in an Fe_2O_3-$FeTiO_3$ intergrowth in the absence of any interaction between the two phases. This model serves as a convenient reference point in the discussion of subsequent simulations. Above 263 K, the magnetocrystalline anisotropy of Fe_2O_3 causes Fe^{3+} spins to lie parallel to the (001) cation layers. Below 263 K, the magnetocrystalline anisotropy constant changes sign (the Morin transition), causing Fe^{3+} spins to align normal to (001). However, substitution of small amounts of Ti into Fe_2O_3 can lead to the suppression of the Morin transition.[27] No evidence for a Morin transition was seen in the present sample using a

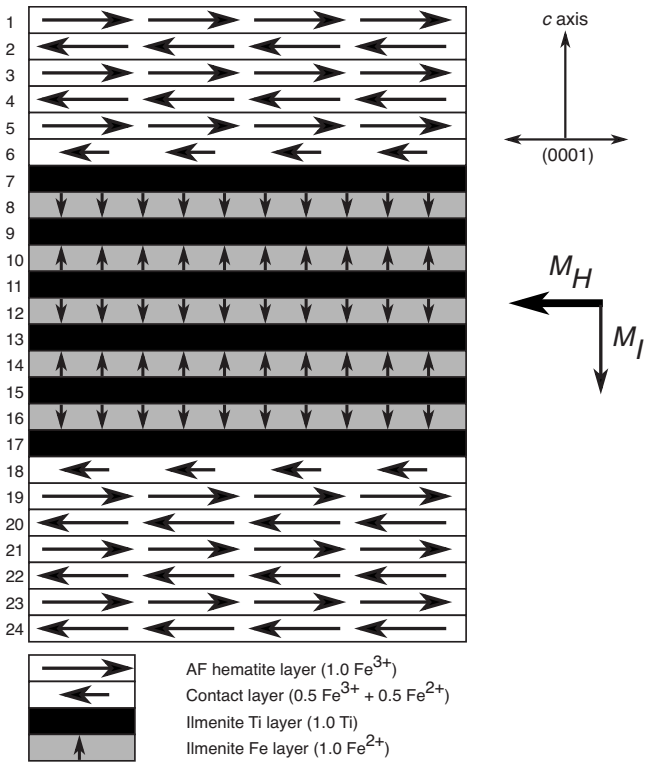

FIG. 3. Idealized model of an $FeTiO_3$ precipitate within an Fe_2O_3 host. Numbered layers correspond to (001) layers of Fe^{3+} (white), Fe^{2+} (gray), and Ti (black) cations. Layers 6 and 18 are contact layers, containing a mixture of Fe^{2+} and Fe^{3+}. M_H is the soft lamellar moment due to imbalance between left and right pointing spins in the Fe_2O_3 host. M_I is the hard lamellar moment due to imbalance between up and down pointing spins in the $FeTiO_3$ host.

combination of Mössbauer spectroscopy and magnetic measurements,[12] nor in any sample of Ti-bearing Fe_2O_3 that has been studied in detail. Therefore, Fe^{3+} spins are expected to prefer to remain parallel to (001) even at low temperature. Strong negative superexchange interactions between adjacent (001) cation layers lead to AFM ordering of Fe^{3+} spins. Each Fe^{3+} spin is rotated by a small angle ($\sim 0.05°$) about the c axis, leading to a small canted moment that lies parallel to (001) and perpendicular to the direction of Fe^{3+} spin alignment.

$FeTiO_3$ has an ordered structure of alternating Fe^{2+} and Ti (001) layers. Inserting paramagnetic $FeTiO_3$ into an Fe_2O_3 host generates a stable defect (or "lamellar") moment due to spin imbalance at the interfaces.[1,8,9] $FeTiO_3$ lamellae are bounded by mixed Fe^{2+}-Fe^{3+} "contact layers." The lamellar moment (labeled M_H in Fig. 3) is parallel to the spin alignment of the contact layers. Reversing the direction of M_H requires switching all the spins in the Fe_2O_3 host, either by coherent rotation within the (001) plane or by driving a domain wall through the system. The required switching field is typically less than 1 T at temperatures greater than 10 K.

$FeTiO_3$ becomes AFM below 55–58 K, with alternating layers of Fe^{2+} spins aligning parallel and antiparallel to the c axis. Lamellae containing an odd number of Fe^{2+} layers will generate an additional contribution to the net moment of the system due to the presence of one layer of uncompensated Fe^{2+} spins (labeled M_I in Fig. 3). M_I may point up or down, depending on the alignment of the Fe^{2+} layers adjacent to the interface. Given the large anisotropy field for switching Fe^{2+} spins (~ 15 T),[28] M_I is unlikely to be reversed by an external field once the Fe^{2+} spins become locked in below 55 K.

From Fig. 3 we can conclude that EB in this system involves exchange coupling between a "soft" AFM phase (Fe_2O_3) and a "hard" AFM phase ($FeTiO_3$), each carrying a net defect moment due to spin imbalance. The dominant uniaxial anisotropy axis for the whole system is parallel to c, but the sign of the anisotropy constant is opposite in each phase, leading to a perpendicular arrangement of spins. This arrangement is distinct from the 90° "spin-flop" coupling discovered by Koon[24] for FM spins in contact with a compensated AFM interface. It should be noted that the spin arrangement depicted in Fig. 3 cannot yield EB. Assuming M_I is fixed, and that the angle between Fe^{2+} and Fe^{3+} spins is exactly 90°, the energy of the system is independent of the in-plane orientation of M_H. That this configuration of spins cannot yield significant exchange bias has been experimentally confirmed for the case of AFM-FM coupling in the system FeF_2-Fe.[29] We postulate that some local realignment of spins close to the Fe_2O_3-$FeTiO_3$ interface is required to yield the observed EB behavior. Our aim here is to investigate possible interface structures within the framework of a classical Heisenberg model, and determine the conditions required to yield EB of the observed magnitude.

III. SETUP OF THE HEISENBERG MODEL

A. Hamiltonian

The magnetic energy of the system is defined as

$$E_{mag} = -\sum_{\langle ij \rangle} J_q^p \boldsymbol{S}_i \cdot \boldsymbol{S}_j + \sum_i K_i (S_i^z)^2 - \sum_i \boldsymbol{B} \cdot \boldsymbol{S}_i. \quad (1)$$

The first term describes the Heisenberg exchange interaction between classical spin vectors $\boldsymbol{S}_i$ and $\boldsymbol{S}_j$ for atoms i and j. Spin vectors of fixed magnitude $S_{3+}=5/2$ and $S_{2+}=4/2$ were used for Fe^{3+} and Fe^{2+} spins, respectively. J_q^p is the exchange constant for a given i-j pair. The label p defines the type of pair (3-3=Fe^{3+}-Fe^{3+}, 2-2=Fe^{2+}-Fe^{2+}, 2-3=Fe^{2+}-Fe^{3+}); q defines the type of interaction (1=1st nearest neighbor, 2=2nd nearest neighbor, etc.). The sum is made over all neighboring atoms i and j, assuming periodic boundary conditions in all three dimensions. The second term describes the uniaxial magnetocrystalline anisotropy, with anisotropy axis parallel to the c axis. K_i is the anisotropy constant for atom i and S_i^z is the c-axis component of spin. Negative values of K_i mean that the anisotropy energy is minimized by maximizing $|S_i^z|$ (i.e., spins prefer to lie either parallel or antiparallel to c). Positive values of K_i mean that the anisotropy energy is minimized by minimizing $|S_i^z|$, forcing spins to lie in the basal plane. The third term describes the effect of an external field, $\boldsymbol{B}$.

Fe_2O_3 is treated as a perfect AFM with no spin canting. At the length scale of interest, the lamellar moment, M_H, makes a much larger contribution to the net moment of the system

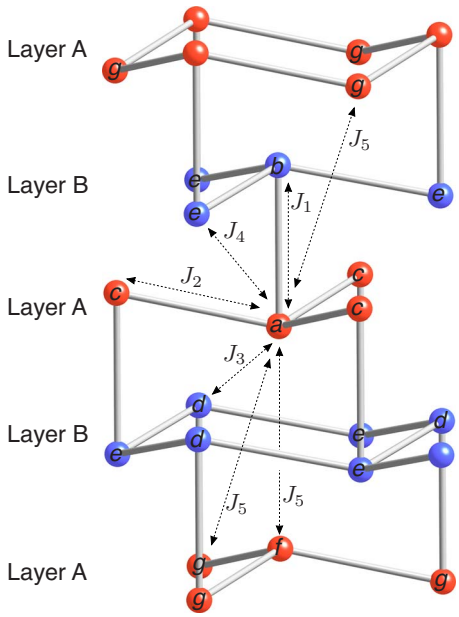

FIG. 4. (Color online) Definitions of the superexchange interaction parameters J_1–J_5 (Table I).

than the canted moment of the Fe_2O_3 host.[30] The anisotropy associated with rotating spins within the (001) plane of Fe_2O_3 is assumed to be negligible in comparison to the anisotropy associated with rotating spins out of the (001) plane.[27] Magnetostatic interaction between Fe_2O_3 and $FeTiO_3$ is assumed to be negligible.

The exchange constants used to model magnetic ordering in Fe_2O_3-$FeTiO_3$ are defined in Fig. 4 and Table I. The majority of the exchange constants are equal to those used by Harrison[1] to model magnetic ordering in the solid solution. However, as noted by the author, the values used by Harrison[1] significantly underestimate the Néel temperature of pure $FeTiO_3$. In order to obtain a more accurate description of magnetic ordering in pure $FeTiO_3$, it was necessary to make two modifications: (i) the definition of the fifth nearest neighbor double-layer interaction (labeled a–f in Fig. 4) was expanded to include six additional pairs of neighbors (labeled a–g in Fig. 4) and (ii) values of the intralayer and double-layer interaction parameters, $J_2^{2\text{-}2}$ and $J_5^{2\text{-}2}$, were adjusted in order to reproduce the correct Néel temperature and transition field for the AFM-FM metamagnetic transition at 4.2 K (8 T).[28] The optimized values of $J_2^{2\text{-}2}=10.77$ K and $J_5^{2\text{-}2}=-0.765$ K (Table I) compare favorably with those determined by Kato *et al.*[28] using a mean-field model.

The single-ion anisotropy of Fe^{2+} is large due to its large unquenched orbital contribution to the magnetic moment.[28] The anisotropy field derived by Kato *et al.*[28] from a mean-field model is 15 T. This translates to a value of $K_{2+}=-6$ K in units appropriate to Eq. (1). This value was confirmed by comparing the experimentally observed perpendicular magnetic susceptibility of $FeTiO_3$ at 4.2 K (0.13 μ_B/cation T)[28] with that obtained from the simulations (0.131 μ_B/cation T). The single-ion anisotropy of Fe^{3+} is at least an order of magnitude smaller than that of Fe^{2+}.[27] As mentioned previously, the sign of the anisotropy constant for pure Fe_2O_3 changes from positive to negative below the Morin transition. Since the current sample does not show a Morin transition, K_{3+} should remain positive at low temperatures. This means that the negative values of K_{3+} observed in pure Fe_2O_3 at low temperature are inappropriate for modeling this system. A value of $K_{3+}=1.2\times10^6$ J/m^3 is quoted for the c-axis anisotropy of Fe_2O_3 at room temperature by Dunlop and Özdemir.[31] Assuming a unit-cell volume of 302 Å^3, and the presence of 12 Fe^{3+} cations per unit cell, this translates to a value of $K_{3+}=0.35$ K/cation. The value of K_{3+} needed to model the system below 60 K, however, is unknown. One estimate for K_{3+} can be obtained from low-temperature studies of Fe_2O_3 nanoparticles, since the Morin transition is suppressed in particles less than 20 nm in diameter.[32] Low-temperature Mössbauer spectroscopy measurements indicate a value of K_{3+} in the range 10^4–10^5 J/m^3.[32,33] This translates to values of K_{3+} in the range 0.003–0.03 K/cation. Below we explore the behavior of the system for $0\leqslant K_{3+}\leqslant 0.35$ K.

B. Simulation configuration

Simulations were performed using an $8\times4\times8$ supercell of the Fe_2O_3 structure in its hexagonal setting, containing 3072 cation positions. The supercell was divided into two $4\times4\times8$ subregions. One subregion was occupied exclusively by Fe^{3+}. Idealized precipitates of pure $FeTiO_3$ in a

TABLE I. Summary of cation-cation interaction types and their chemical and magnetic interaction parameters.

Interaction type (q)	Cation pair (see Fig. 4 for definitions)	Cation-cation distance (Å)	Number of interactions per cation	Inter-intra-double-layer interaction	Octahedral sharing	Cation-oxygen-cation bond angle (°)	Magnetic interaction parameter (K) 3-3=Fe^{14}-Fe^{14} 2-2=Fe^{24}-Fe^{24} 2-3=Fe^{24}-Fe^{14}		
							$J_q^{3\text{-}3}$	$J_q^{2\text{-}2}$	$J_q^{2\text{-}3}$
1	a-b	2.9	1	Interlayer	Face	86.5	10.2	2.55	6.375
2	a-c	2.971	3	Interlayer	Edge	93.9	2.72	10.77	1.7
3	a-d	3.36	3	Interlayer	Corner	119.7	−50.49	−12.62	−31.55
4	a-e	3.71	6	Interlayer	Corner	131.6	−39.44	−9.86	−24.65
5	a-f, a-g	3.99, 5.43	1.6	Double	None	NA	−1.7	−0.765	−1.06

host of pure Fe_2O_3 were created in the adjacent subregion, according to the layering schemes defined by Robinson *et al.*[30,34] "Odd" precipitates contain five Fe^{2+} layers alternating with six Ti layers, and are bounded by two contact layers containing an equal mixture of Fe^{2+} and Fe^{3+} (e.g., Fig. 3). Cations within the contact layers were ordered according to the scheme predicted by Harrison[1] and Robinson *et al.*[34] "Even" precipitates contain four Fe^{2+} layers alternating with five Ti layers, and are bounded by two contact layers.

C. Simulation algorithm

At equilibrium, a given configuration of spins will occur with a thermodynamic probability determined by the temperature, T, and the Boltzmann distribution, $\exp(-E_{mag}/T)$, where both E_{mag} and T are measured in Kelvin (Table I). In a Monte Carlo simulation, the equilibrium thermodynamic properties are determined by averaging over a number of spin configurations generated with their correct thermodynamic probability. The supercell is generated with an arbitrary starting configuration. During each Monte Carlo step, an atom is chosen at random and its spin is rotated by a randomly chosen angle, ϕ, about a randomly chosen direction (normal to the original spin vector). ϕ is restricted to lie in the range $0<\phi<2\pi f$, where $0<f\leqslant 1$. If the change in energy, ΔE_{mag}, is negative, then the rotation is accepted. If ΔE_{mag} is positive, then the rotation is accepted with a probability $\exp(-\Delta E_{mag}/T)$. The value of f is adjusted to ensure that a reasonable ratio of accepted to rejected steps is obtained (a value of $f=0.1$ was used in all the following simulations).[35] After a sufficient number of steps the system reaches equilibrium, with configurations generated independently of the starting configuration. The equilibrium properties (energy, degree of magnetic order, etc.) can then be determined by averaging over a number of steps until the desired statistical significance is reached. The total number of steps used in each simulation was 8×10^7, which included an initial equilibration run of 4×10^7 steps followed by a production run of 4×10^7 steps.

IV. RESULTS

A. Spin structure of odd-layered precipitates

Monte Carlo simulations were performed as a function of K_{3+} in order to investigate the range of possible interface spin structures. The starting configuration was an $8\times4\times8$ supercell of Fe_2O_3 containing an $FeTiO_3$ precipitate with an odd number of Fe^{2+} layers. A detailed snapshot of the interface structure obtained for $K_{3+}=0.1$ K is shown in Fig. 5(a). The system was first equilibrated at $T=10$ K for 8×10^7 steps and then at $T=0$ K for $\sim1\times10^5$ steps. The latter simulation eliminates thermal fluctuations, allowing the details of the magnetic structure to be examined more easily. The $FeTiO_3$ precipitate can be split into two distinct regions: an antiferromagnetic core [shaded orange in Fig. 5(a)] and a ferromagnetic rim [shaded green in Fig. 5(a)]. The core region adopts the same antiferromagnetic structure as bulk $FeTiO_3$, with Fe^{2+} spins aligned strictly parallel and antiparallel to c. Of the five Fe^{2+} layers in the core region, three are pointing down and two are pointing up, leading to a net downward-pointing spin (labeled M_I). This net spin is rigidly coupled to the c axis by the large negative value of K_{2+}.

The uppermost and lowermost Fe^{2+} layers in the core region both point down (i.e., they are "in phase"). The equilibrium orientation of the neighboring contact-layer spins is determined by the balance between competing exchange and anisotropy energies. The contact layers are coupled antiferromagnetically to the neighboring Fe^{2+} layers via the double-layer interactions J_5 [Table I; dotted lines in Fig. 5(a)]. It is energetically favorable, therefore, for spins in both contact layers to point vertically upward. This orientation is also favored by the negative anisotropy of contact-layer Fe^{2+} spins. It is made energetically unfavorable, however, by the positive anisotropy of the Fe^{3+} spins in the contact layers. The result of this energy balance is that the contact-layer spins are tilted out of the basal plane by roughly 45°. Since the contact layers are strongly coupled to the Fe^{3+} spins of the Fe_2O_3 host via the antiferromagnetic interactions J_3 and J_4 [Table I, solid lines in Fig. 5(a)], the host Fe^{3+} spins are also forced to tilt out of the basal plane. This tilting is expected to gradually decay with distance from the interface. The extent to which the tilting propagates into the Fe_2O_3 host as one moves away from the interface will be a function of both the exchange length of Fe_2O_3 (~2 μm) and the relative position of surrounding precipitates.

The contact layers form the top and bottom of the ferromagnetic rim region. This rim results from the mismatch in periodicity of the $FeTiO_3$ and Fe_2O_3 magnetic structures (Fe_2O_3 has a two-layer repeat, whereas $FeTiO_3$ has a four-layer repeat due to the intervening Ti layers), which means that all Fe^{2+} layers in the $FeTiO_3$ precipitate coincide in position with upward-pointing layers in the Fe_2O_3 host. In a downward-pointing Fe^{2+} layer, the Fe^{2+} spin immediately adjacent to the interface is flipped by exchange interactions with the adjacent host. Of the five Fe^{2+} layers in Fig. 5(a) there are three such "conflicted" Fe^{2+} layers and two "unconflicted." The net spin of the ferromagnetic rim (labeled M_H) points up and to the right, and is held in place by antiferromagnetic interaction with the Fe^{2+} spins of the core $FeTiO_3$ region. Unlike the situation depicted in Fig. 3, there is now a substantial component of M_H that is antiparallel to M_I, making EB a possibility.

A plot of the z component of spin as a function of K_{3+} (Fig. 6) reveals two threshold values (indicated by the dashed lines). For $K_{3+}\geqslant0.225$ K, Fe^{3+} spins (and also the Fe^{2+} spins in the contact layers) lie in the basal plane, as in bulk Fe_2O_3 above the Morin transition. For $K_{3+}\leqslant0.05$ K these spins lie exactly parallel and antiparallel to c, as in bulk Fe_2O_3 below the Morin transition. For $0.05<K_{3+}<0.225$ K, these spins make an intermediate angle to the basal plane. Such intermediate spin directions have been reported in Fe_2O_3 nanoparticles at low temperatures using Mössbauer spectroscopy, and are similarly thought to be the result of exchange coupling across the interface between adjacent particles.[33,36,37] On this basis we would expect EB to exist only when the anisotropy of the Fe_2O_3 host is less than the critical threshold $K_{3+}=0.225$ K. As discussed below, this threshold is not a universal constant, but varies with the separation of the $FeTiO_3$ lamellae, and is therefore likely to

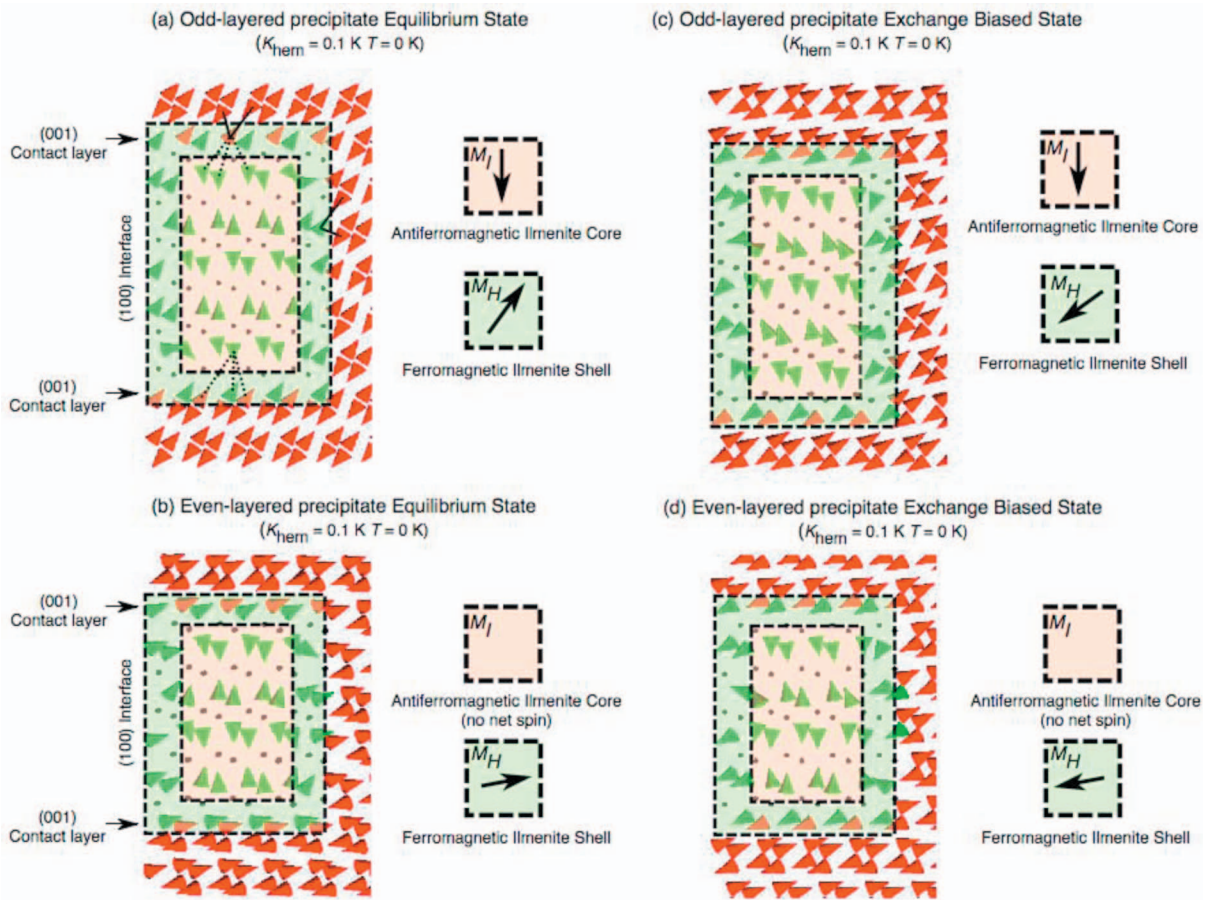

FIG. 5. (Color) Interface magnetic structures for odd-layered [(a) and (c)] and even-layered [(b) and (d)] $FeTiO_3$ precipitates in an Fe_2O_3 host. The red and green cones indicate the direction of spin on Fe^{3+} and Fe^{2+} cations, respectively. Ti cation positions are indicated by the black dots. (a) Equilibrium structure for an odd-layered precipitate in zero field. The central core of the $FeTiO_3$ precipitate (shaded light orange) carries a net downward spin (M_I). The outer rim (shaded green) adopts a ferromagnetic structure with net spin (M_H) at ~45° to the basal plane. The presence of strong antiferromagnetic interactions across (100) and (001) interfaces are indicated by the solid black lines. Exchange coupling between the ferromagnetic rim and the ilmenite core is governed by weaker antiferromagnetic interactions $J_5^{2\text{-}3}$ and $J_5^{2\text{-}2}$ across the (001) interfaces (indicated by the dotted lines). (b) Equilibrium structure for an even-layered precipitate in zero field. M_I is zero and M_H lies much closer to the basal plane for an even-layered precipitate. Tilting M_H out of plane leads to antiferromagnetic alignment of spins across one (001) interface and ferromagnetic alignment of spins across the bottom interface. (c) Exchange biased state of an odd-layered precipitate obtained in a field of −3 T applied along [001]. The vertical component of the contact-layer spins are brought into ferromagnetic alignment with the Fe^{2+} spins of the central core. This leads to a larger net spin in the exchange biased state and a vertical shift of the hysteresis loop. (d) Exchange biased state of an even-layered precipitate. This state is degenerate with that shown in (b).

vary from sample to sample, or from region to region within a given sample.

B. Spin structure of even-layered precipitates

A detailed snapshot of the interface structure obtained for an even-layered precipitate with K_{3+}=0.1 K is shown in Fig. 5(b). The two key differences are that (a) there are equal numbers of up and down layers in the core region (M_I=0) and (b) the uppermost and lowermost Fe^{2+} layers of the core region are out of phase. The upper contact layer is driven to tilt upward by antiferromagnetic exchange interaction with the uppermost Fe^{2+} layer of the core. Such tilting, however, would cause the lower contact layer to tilt into ferromagnetic alignment with the lowermost Fe^{2+} layer of the core. The exchange interactions at the two interfaces cannot be satisfied simultaneously (a type of frustration), leading to a compromise solution whereby the out-of-plane tilting of the ferromagnetic rim is drastically reduced. On this basis, even-layered precipitates would not be expected to contribute to the EB.

C. Field dependence of the interface structure

The field dependence of the interface structure was investigated for a range of applied field directions and K_{3+} values. The system was first equilibrated in a saturating field in the chosen direction. The final spin configuration of the equilibration run was then used as the starting configuration for the next simulation with slightly reduced amplitude of applied field. This procedure was repeated until the field reached zero, after which the field was increased in the opposite di-

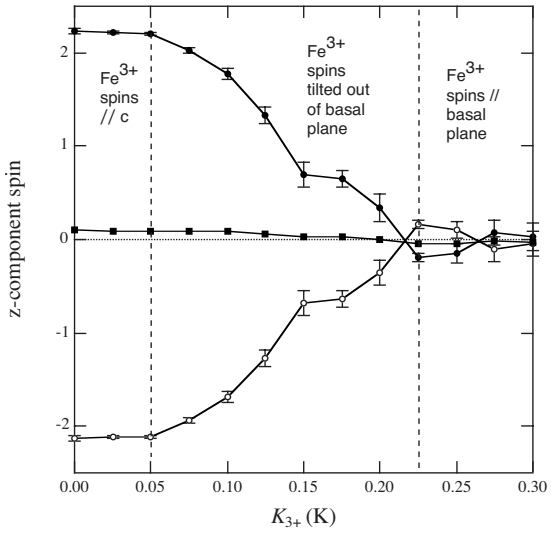

FIG. 6. Average component of spin along z on odd and even numbered layers of the simulation cell (closed and open circles, respectively) and the net spin along z (squares) as a function of K_{3+}. All simulations performed at $T=10$ K. For $K_{3+}>0.225$ K, all Fe^{3+} spins (and also the Fe^{2+} spins within the contact layers) lie in the basal plane. The net spin along z is negative due to the contribution from the Fe^{2+} spins of the $FeTiO_3$ precipitate (M_I). For $K_{3+}<0.05$ K the Fe^{3+} spins and the contact-layer Fe^{2+} spins lie parallel and antiparallel to z.

rection until the negative saturation state was reached. The whole procedure was then repeated in reverse until the system returned to positive saturation. In this way the system is driven stepwise through a full hysteresis cycle, enabling the path taken during reversal to be observed, and the magnitude of any exchange bias to be estimated (Figs. 7 and 8).

Figure 7(a) shows the hysteresis loop obtained for an odd-layered precipitate with $K_{3+}=0.1$ K, $T=10$ K, and field applied along the c axis. The initial equilibration was performed with a positive field of 3 T. The net moment (M_H+M_I) in the equilibrated state makes an angle of ~35° to the basal plane [closed red circle in Fig. 8(a)]. The spin structure is identical to that illustrated in Fig. 5(a), with M_I pointing down and M_H pointing up and to the right. This configuration brings the vertical component of the contact-layer spins into antiferromagnetic alignment with the core Fe^{2+} spins and leads to a partial cancellation of the vertical component of the net moment. The coercive field for the initial reversal path is −1.3 T. Reversal occurs via coherent rotation of the host Fe^{3+} spins, with the ferromagnetic rim (M_H) remaining parallel to the host spins at all times. The antiferromagnetic core (M_I) remains unchanged throughout. The path taken by the net moment during reversal is indicated by the solid arrows in Fig. 8(a). The final spin structure obtained in a field of −3 T is shown in Fig. 5(c) [referred to as the "exchange biased state" in Fig. 8(a)]. M_H now points down and to the left, bringing the vertical component of the contact-layer spins into ferromagnetic alignment with the core Fe^{2+} spins. Since this is energetically unfavorable, the degree of out-of-plane tilting in the exchange biased state is significantly less than in the equilibrium state. The high energy of the exchange biased state is lessened slightly by the reduction in the number of conflicted Fe^{2+} layers from three to two [cf. Figs. 5(a) and 5(c). The vertical components of M_H and M_I now reinforce each other, yielding a larger net moment in the exchange biased state than the equilibrium state, and a corresponding vertical shift of the hysteresis loop. Such vertical shifts have been observed in other systems exhibiting giant EB.[38] The coercive field for the return path is −0.5 T, yielding a horizontal shift of −0.9 T, similar in magnitude to that observed EB shift in Fig. 1(d). The path taken by the net moment during the return path is significantly different from that of the initial path [dashed arrow in Fig. 8(a)].

Figure 7(b) shows the hysteresis loop for fields applied at 45° to the c axis [i.e., directed along M_H in Fig. 5(a)]. In this case, the simulations were started with the system in the exchange biased state. The paths taken during the transformation from exchange biased to equilibrium state, and vice versa, are similar to those observed for fields applied along c [Figs. 8(a) and 8(b)]. The difference in initial and return paths leads to a highly asymmetric loop with a horizontal shift of −0.52 T. The vertical shift is also present, but less pronounced than for fields applied along c.

EB is drastically reduced for fields applied normal to the c axis [Fig. 7(c)]. In this case, reversal occurs by the precession of M_H about the c axis [Fig. 8(c)]. The vertical component of M_H remains positive, and the equilibrium spin configuration is maintained throughout. Since in-plane anisotropy has been neglected in this model, the energy of the system is cylindrically symmetric about the c axis, and the start and end points of the hysteresis loop are degenerate. The application of large fields normal to c causes the net moment to lie very close to the basal plane [Fig. 8(c)]. This contrasts with the behavior observed for fields along c, where the net moment makes a large angle to the c axis [Fig. 8(a)].

EB is also drastically reduced for even-layered precipitates [Fig. 7(d)]. Although the vertical component of M_H is switched during the reversal [Fig. 8(d)], the exchange biased configuration is the exact reverse of the equilibrium configuration [Fig. 5(d)].

The coercivities obtained during these simulations are typically much larger than those observed in the natural sample. This discrepancy can be explained by the different magnetic switching mechanisms: switching is achieved via coherent rotation of spins in the simulations, but is more likely to be achieved by driving domain walls through the Fe_2O_3 host in a real sample. The simulations represent a highly idealized model of interface, and provide some insight into the possible interface magnetic structure. The real sample contains a distribution of lamellar sizes, separations, and orientations, making any direct comparison of simulated and observed hysteresis loops difficult. It is satisfying, nevertheless, that the magnitude of EB field can be reproduced with physically reasonable values of the exchange and anisotropy constants.

V. DISCUSSION

The Monte Carlo simulations indicate that EB is expected only when there is appreciable tilting of the Fe_2O_3 spins out

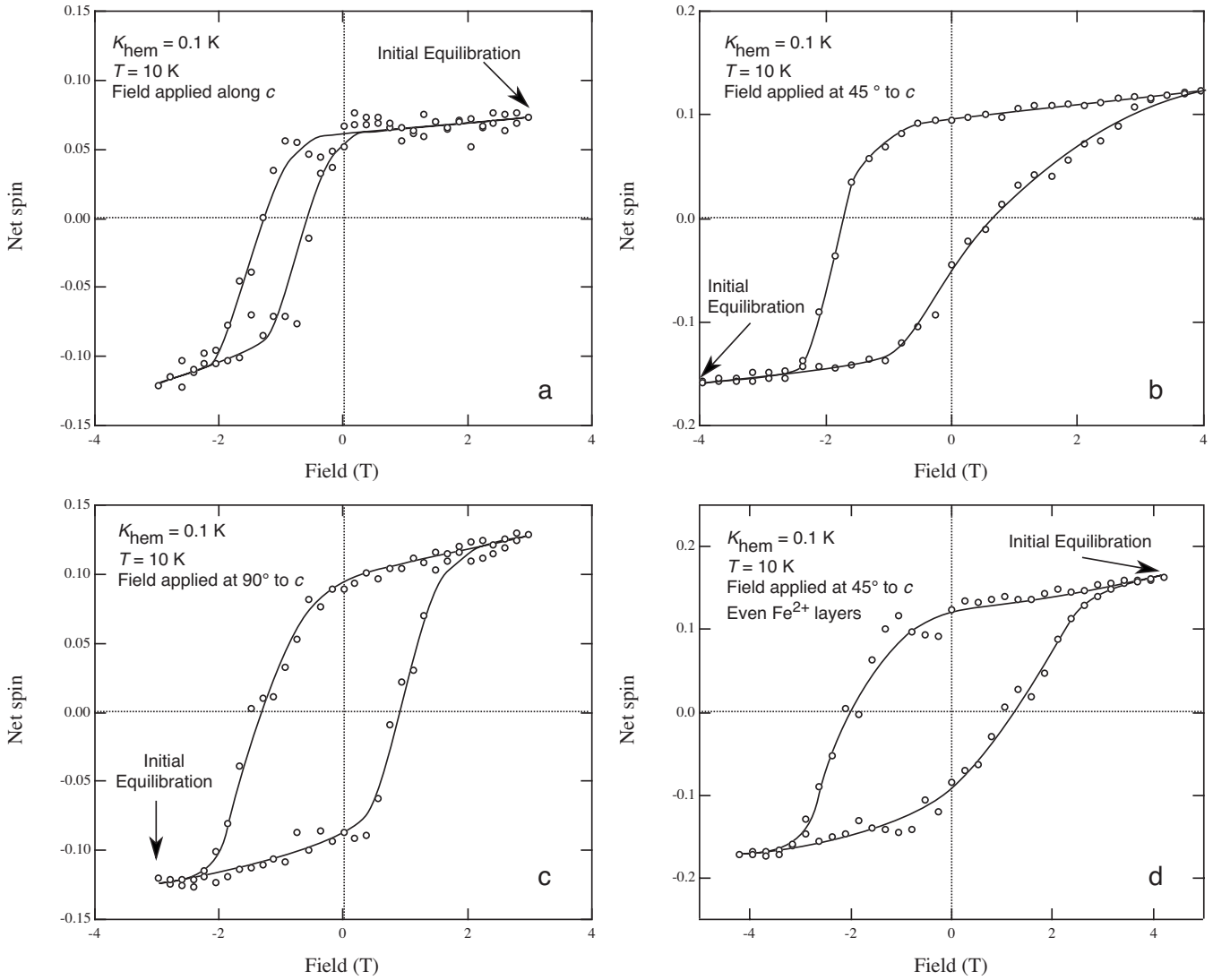

FIG. 7. Simulated hysteresis loops for a variety of applied field directions. Each data point represents the result of 8×10^7 Monte Carlo steps (4×10^7 equilibration plus 4×10^7 production steps). The arrows indicate the starting point for the simulations. The net spin is defined as the component parallel to the direction of applied field. (a) An odd-layered $FeTiO_3$ precipitate with K_{3+}=0.1 K, T=10 K, and field applied along c. (b) An odd-layered $FeTiO_3$ precipitate with K_{3+}=0.1 K, T=10 K, and field applied at 45° to c. (c) An odd-layered $FeTiO_3$ precipitate with K_{3+}=0.1 K, T=10 K, and field applied at 90° to c. (d) An even-layered $FeTiO_3$ precipitate with K_{3+}=0.1 K, T=10 K, and field applied at 45° to c.

of the basal plane (i.e., for small K_{3+}). Here we develop a simple model that will allow us to make some quantitative predictions regarding the likelihood of such out-of-plane tilting in a given sample.

The system is considered as a simplified intergrowth of Fe_2O_3 and $FeTiO_3$, interacting only via their (001) interfaces, and with periodic boundary conditions in all three dimensions (as in Fig. 3). M_I is assumed to remain fixed, while M_H (determined by the orientation of Fe^{3+} and Fe^{2+} spins in the host and contact layers) makes an angle, θ, to the c axis. The energy of the system in zero applied field can be written as

$$E_{mag} = -J_{int}\cos\theta + K_{av}\cos^2\theta, \tag{2}$$

where J_{int} is a constant describing the strength of the exchange interaction between the contact layers and the neighboring Fe^{2+} layers as follows:

$$J_{int} = 4S_{2+}^2 J_5^{2-2} + 3S_{2+}S_{3+}J_5^{2-3} = 28.2\ \text{K} \tag{3}$$

and K_{av} is a constant describing the combined anisotropy energy associated with rotating the Fe^{3+} and Fe^{2+} spins in the Fe_2O_3 host and two contact layers as follows:

$$K_{av} = (N+1)K_{3+}S_{3+}^2 + K_{2+}S_{2+}^2. \tag{4}$$

N is the number of Fe^{3+} layers in the host (not including the contact layers). The equilibrium orientation of M_H is then

$$\cos\theta = \frac{J_{int}}{2K_{av}}. \tag{5}$$

Combining Eqs. (4) and (5) we note that $\theta\to90°$ (i.e., M_H lies in the basal plane) when K_{av} is large (i.e., when $N\to\infty$). Hence, if precipitates are widely spaced, M_H is expected to

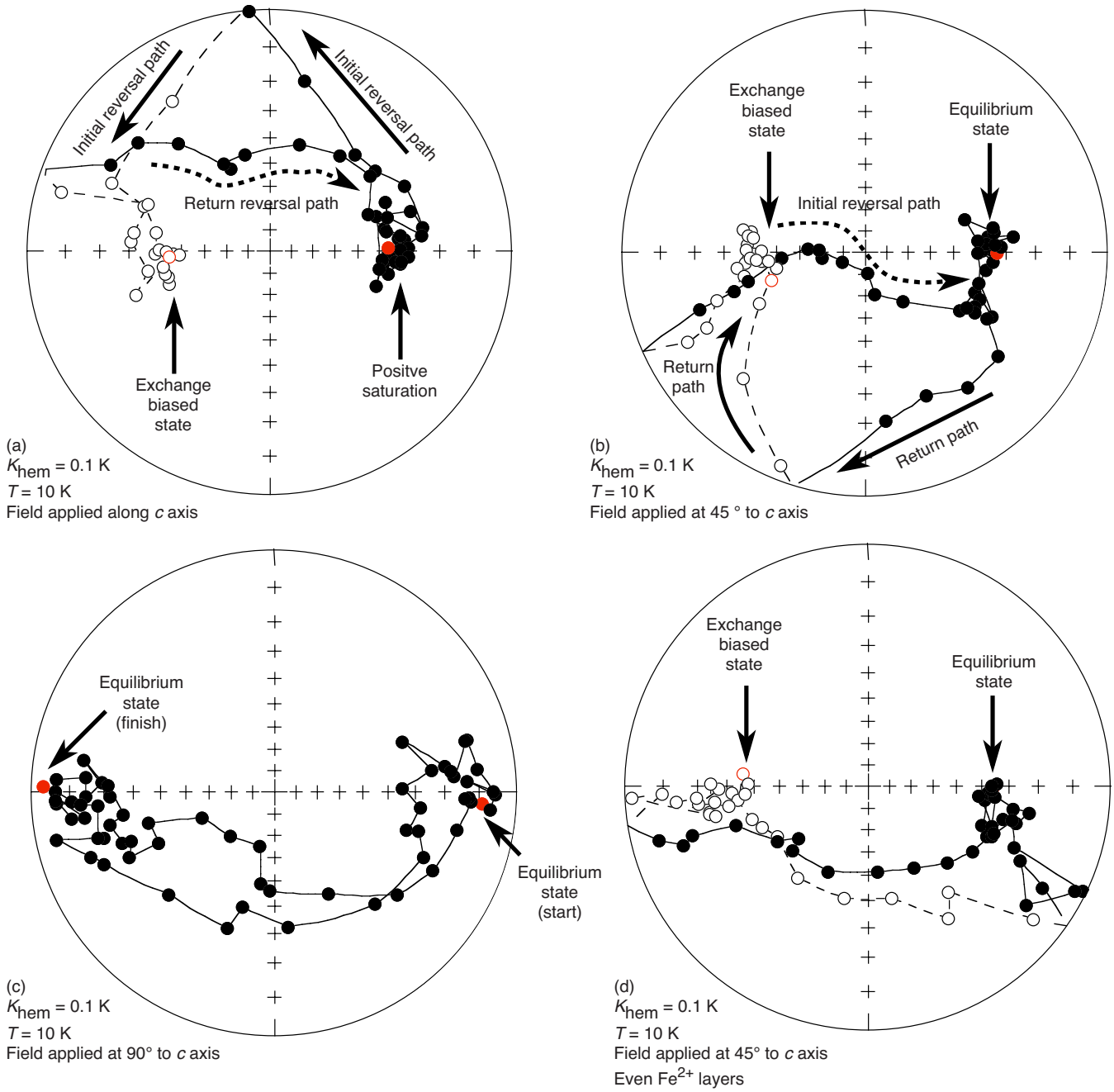

FIG. 8. (Color online) Upper hemisphere stereographic projections showing the path taken by the net spin vector during the magnetization reversal process. Each figure was derived from the corresponding hysteresis loop data shown in Fig. 7. The closed and open symbols represent net magnetization vectors pointing upward and downward, respectively.

lie in the basal plane, even if K_{3+} is small. Conversely, if precipitates are very closely spaced, M_H is expected to be tilted out of plane, even if K_{3+} is large. M_H points exactly along c when $K_{av} \leqslant J_{int}/2$. Assuming a value of $K_{3+} = 0.35$ K, equivalent to the known room-temperature value for bulk Fe_2O_3,[31] the critical value of $(N+1)$ below which M_H points exactly along c is 17.4. This corresponds to ~3 unit cells of Fe_2O_3, or a separation of 4.2 nm—a similar order of magnitude to the spacing of lamellae visible in Fig. 2(c). If $K_{3+} < 0.35$ K, then tilting may also be favorable for more widely spaced lamellae. Assuming a value of $K_{3+} = 0.03$ K, equal to the upper limit observed in 9 nm diameter nanoparticles of Fe_2O_3,[33] a critical value of $(N+1)=203$ is obtained, equivalent to a separation of 47 nm.

Although an approximation, this calculation does illustrate that some degree of out-of-plane tilting is a realistic proposition in this sample, especially in the regions of Fe_2O_3 sandwiched between closely spaced $FeTiO_3$ precipitates. The calculation also provides a possible explanation for why exchange bias of this magnitude is not observed in all intergrowths of Fe_2O_3 and $FeTiO_3$: only those samples where K_{3+} is small enough (and the nanoscale lamellae close enough) to

produce appreciable out-of-plane tilting will display giant exchange bias.

ACKNOWLEDGMENTS

This research was supported by grants from the Research Council of Norway (Grant No. 163556 "The nature and origin of natural magnetic nanoscale materials" and grant No. 169470 to S.A.M.), by a NERC Advanced Fellowship (NE/B501339/1 "Mineral magnetism at the nanometre scale" to R.J.H.), and by the European Science Foundation under the EUROCORES program EuroMinScI, through Contract No. ERAS-CT-2003-980409 of the European Commission, DG Research, FP6. The authors would like to thank K. Fabian for his contribution to the discussion of the interface exchange bias energy.

*rjh40@esc.cam-ac.uk

[1] R. J. Harrison, Am. Mineral. **91**, 1006 (2006).
[2] S. A. McEnroe, R. J. Harrison, P. Robinson, U. Golla, and M. J. Jercinovic, J. Geophys. Res. **106**, 30523 (2001).
[3] S. A. McEnroe, R. J. Harrison, P. Robinson, and F. Langenhorst, Geophys. J. Int. **151**, 890 (2002).
[4] S. A. McEnroe, F. Langenhorst, P. Robinson, G. Bromiley, and C. Shaw, Earth Planet. Sci. Lett. **226**, 175 (2004).
[5] S. A. McEnroe, L. L. Brown, and P. Robinson, J. Appl. Geophys. **56/3**, 195 (2004).
[6] S. A. McEnroe, J. R. Skilbrei, P. Robinson, F. Heidelbach, F. Langenhorst, and L. L. Brown, Geophys. Res. Lett. **31**, L19601 (2004).
[7] T. Kasama, S. A. McEnroe, N. Ozaki, T. Kogure, and A. Putnis, Earth Planet. Sci. Lett. **224**, 461 (2004).
[8] P. Robinson, R. J. Harrison, S. A. McEnroe, and R. B. Hargraves, Nature (London) **418**, 517 (2002).
[9] P. Robinson, R. J. Harrison, S. A. McEnroe, and R. B. Hargraves, Am. Mineral. **89**, 725 (2004).
[10] Y. Ishikawa and Y. Syono, J. Phys. Chem. Solids **24**, 517 (1963).
[11] R. J. Harrison, T. Kasama, T. A. White, E. T. Simpson, and R. E. Dunin-Borkowski, Phys. Rev. Lett. **95**, 268501 (2005).
[12] S. A. McEnroe, B. Carter-Stiglitz, R. H. Harrison, P. Robinson, K. Fabian, and C. McCammon, Nat. Nanotechnol. **2**, 631 (2007).
[13] J. Dho, C. W. Leung, Z. H. Barber, and M. G. Blamire, Phys. Rev. B **71**, 180402(R) (2005).
[14] S. Bae, J. H. Judy, W. F. Egelhoff, and P. J. Chen, J. Appl. Phys. **87**, 6650 (2000).
[15] J. Nogués and I. Schuller, J. Magn. Magn. Mater. **192**, 203 (1999).
[16] K. Fabian (private communication).
[17] W. H. Meiklejohn and C. P. Bean, Phys. Rev. **105**, 904 (1957).
[18] A. E. Berkowitz and K. Takano, J. Magn. Magn. Mater. **200**, 552 (1999).
[19] T. C. Schulthess and W. H. Butler, Phys. Rev. Lett. **81**, 4516 (1998).
[20] T. C. Schulthess and W. H. Butler, J. Appl. Phys. **85**, 5510 (1999).
[21] M. Kiwi, J. Magn. Magn. Mater. **234**, 584 (2001).
[22] R. Stamps, J. Phys. D **33**, R247 (2000).
[23] J. Nogués, J. Sort, V. Langlais, V. Skumryev, S. Suriñach, J. S. Muñoz, and M. D. Baró, Phys. Rep. **422**, 65 (2005).
[24] N. C. Koon, Phys. Rev. Lett. **78**, 4865 (1997).
[25] D. Mauri, H. C. Siegmann, P. S. Bagus, and E. Kay, J. Appl. Phys. **62**, 3047 (1987).
[26] A. P. Malozemoff, Phys. Rev. B **35**, 3679 (1987).
[27] A. H. Morrish, *Canted Antiferromagnetism: Hematite* (World Scientific Singapore, 1994).
[28] H. Kato, M. Yamada, H. Yamuchi, H. Hiroyoshi, H. Takei, and H. Watanabe, J. Phys. Soc. Jpn. **51**, 1769 (1982).
[29] J. Nogués, T. J. Moran, D. Lederman, I. K. Schuller, and K. V. Rao, Phys. Rev. B **59**, 6984 (1999).
[30] P. Robinson, F. Heidelbach, A. M. Hirt, S. A. McEnroe, and L. L. Brown, Geophys. J. Int. **165**, 17 (2006).
[31] D. J. Dunlop and Ö. Özdemir, *Rock Magnetism: Fundamentals and Frontiers* (Cambridge University Press, Cambridge, 1997).
[32] F. Bødker, M. F. Hansen, C. B. Koch, K. Lefmann, and S. Mørup, Phys. Rev. B **61**, 6826 (2000).
[33] C. Frandsen and S. Mørup, Phys. Rev. Lett. **94**, 027202 (2005).
[34] P. Robinson, R. J. Harrison, and S. A. McEnroe, Am. Mineral. **91**, 67 (2006).
[35] H. Kachkachi, A. Ezzir, M. Nogués, and E. Tronc, Eur. Phys. J. B **14**, 681 (2000).
[36] S. H. Gee, Y. K. Hong, J. C. Sur, D. W. Erickson, M. H. Park, and F. Jeffers, IEEE Trans. Magn. **40**, 2691 (2004).
[37] C. Frandsen and S. Mørup, J. Magn. Magn. Mater. **266**, 36 (2003).
[38] R. K. Zheng, G. H. Wen, K. K. Fung, and X. X. Zhang, J. Appl. Phys. **95**, 5244 (2004).